Nonlinear mode coupling and resonant excitations in two-component Bose-Einstein condensates

Ju-Kui Xue,* Guan-Qiang Li, Ai-Xia Zhang, and Ping Peng
College of Physics and Electronics Engineering, Northwest Normal University, Lanzhou, 730070, China
(Received 1 October 2007; revised manuscript received 13 November 2007; published 24 January 2008)

Nonlinear excitations in two-component Bose-Einstein condensates (BECs) described by two coupled Gross-Pitaevskii equations are investigated analytically and numerically. The beating phenomenon, the higher-harmonic generation, and the mixing of the excited modes are revealed by both variational approximation and numerical method. The strong excitations induced by the parametric resonance are also studied by time-periodic modulation for the intercomponent interaction. The resonance conditions in terms of the modulation frequency and the strength of intercomponent interaction are obtained analytically, which are confirmed by numerical method. Direct numerical simulations show that, when the resonance takes place, periodic phase separation and multisoliton configurations (including soliton trains, soliton pairs, and multidomain walls) can be excited. In particular, we demonstrate a method for formation of multisoliton configurations through parametric resonance in two-component BECs.

DOI: 10.1103/PhysRevE.77.016606 PACS number(s): 05.45.Yv, 03.75.−b

I. INTRODUCTION

Two-component Bose-Einstein condensates (BECs) produced experimentally by simultaneously trapping atoms in distinct hyperfine or spin levels or of different species are described by the two coupled Gross-Pitaevskii equations (GPEs). The extra internal degrees of freedom introduced by the multiple components interaction leads to rich phenomena and complex dynamics in two-component BECs. Among them, multimode collective excitations [1–7], solitons (or soliton trains and soliton pairs) [8–17], and multidomain walls [18–21] are fundamental and important issues. Because of strong nonlinear coupling, complex excitation spectra and mixing of excited modes [1,2], rich dynamics of the center-of-mass oscillation [3–6], quadruple and scissors modes, and second-harmonic generation [7] are revealed in two-component BECs. While many studies about the collective excitations in two-component BECs have been made, many important issues for the collective excitations of two-component BECs remain to be investigated. The beating phenomenon, the higher-harmonic generation, and the mixing properties of oscillation modes in two-component BECs have not been studied. These will be one of the main contents of this work. By using the variational method, the mode coupling and mixing, the beating phenomenon, and the second- and even higher-harmonic modes are predicted analytically. In addition, our theoretical results are confirmed by direct numerical integration of the full GPEs.

Solitons (soliton trains and soliton pairs) [8–17] and multidomain walls [18–21] are important strong excitations in two-component BECs. It is believed that solitary wave and multidomain formation are all related to the modulational instability induced by the coupling between the two condensates. In experiments, the multisoliton configurations can be generated by various methods, e.g., by imprinting spatial phase distribution for the initial wave packet [22], or by inducing small density defects with an extended slow light technique in a condensate [23]. Here, we want to demonstrate a method for formation of multisoliton configurations (including soliton trains, soliton pairs, and multidomain walls) in two-component BECs by external parametric excitation. Parametric excitation corresponds to the exponential growth of certain modes of the system induced by the periodic variation of a parameter. It is a very general phenomenon occurring in a nonlinear system and, especially, in BEC [24–28]. Parametric excitation induced by temporal periodic modulation of atomic scattering length can result in the generation of Faraday waves [29] and solitons [26,30,31] in one-component BEC. However, the parameter excitations in two-component BECs have not been investigated until now. By modulating the intercomponent interaction periodically (experimentally, this can be easily done by the Feshbach resonance technique [32]), we obtain analytically the resonance conditions in terms of the modulating frequency and the strength of intercomponent interaction. The analytical results are confirmed by our numerical integrating of the fully coupled GPEs. Furthermore, our direct numerical results reveal very rich parametric excitations in two-component BECs, such as periodic phase separation, dark-dark soliton trains, dark-bright soliton pairs, periodic appearance of multidomain walls, and long lived multidomain walls. These results have not been reported previously. We believe these results are very significant for investigating the topological excitations in two-component BECs.

The paper is organized as follows. In Sec. II, we first give the basic model for the coupled two-component BECs system. In Sec. III, the harmonic generation and nonlinear coupling of oscillation modes are investigated by both variational analysis and numerical method. The parametric resonance induced by modulating the intercomponent interaction periodically is presented in Sec. IV. Subsequently, the formation of multisoliton states are obtained numerically, in particular, a method for generation of multisoliton configurations in two-component BECs is presented, which can readily be put into practice in current experiments. Section V summarizes our conclusions.

*xuejk@nwnu.edu.cn

II. BASIC MODEL

We assume that the wave functions $\Phi_k(\mathbf{r},t)$ $(k=1,2)$ characterize the two condensates in our system. At very low temperature, the total energy functional of the system is

$$E=\int d\mathbf{r}\left[\sum_{k=1}^{2}\left(\frac{\hbar^2}{2m_k}|\nabla\Phi_k|^2+V_{ext}^{(k)}|\Phi_k|^2+\frac{g_k}{2}|\Phi_k|^4\right)+g_{12}|\Phi_1|^2|\Phi_2|^2\right], \tag{1}$$

with the axisymmetric harmonic trapping potentials

$$V_{ext}^{(k)}(\mathbf{r})=\frac{1}{2}m_k(\omega_k^2x^2+\omega_{k\perp}^2r^2), \tag{2}$$

where the nonlinear coupling constants $g_k=4\pi\hbar^2a_k/m_k$ and $g_{12}=2\pi\hbar^2a_{12}/m_{12}$, the reduced mass $m_{12}=m_1m_2/(m_1+m_2)$.

The dynamics of two-component BECs can be described by the coupled GPEs, which are derived from the variational principle $i\hbar\,\partial\Phi_k/\partial t=\delta E/\delta\Phi_k^*$ as

$$i\hbar\frac{\partial\Phi_k}{\partial t}=\left[-\frac{\hbar^2\nabla^2}{2m_k}+V_{ext}^{(k)}+g_k|\Phi_k|^2+g_{12}|\Phi_{3-k}|^2\right]\Phi_k. \tag{3}$$

The normalization of each wave function is taken independently as $\int d\mathbf{r}|\Phi_k(\mathbf{r},t)|^2=N_k$, and the total particle number $N=N_1+N_2$. When $\omega_k/\omega_{k\perp}\ll 1$, the potentials can be regarded as cigar-shaped trapping geometries. In this case, we can factorize the condensates wave functions into a longitudinal and a transverse part as

$$\Phi_k(\mathbf{r},t)=\varphi_{k\perp}(y,z)\psi_k(x,t)e^{-i\omega_{k\perp}t}, \tag{4}$$

where $\varphi_{k\perp}(y,z)=\exp[-(y^2+z^2)/2b_{k\perp}^2]/\sqrt{\pi}b_{k\perp}$ are the normalized ground state wave functions of the harmonic oscillator in the transverse direction, with $b_{k\perp}=\sqrt{\hbar/m_k\omega_{k\perp}}$ being the corresponding characteristic lengths. Inserting the factorized expressions into Eq. (3), and integrating it over the transverse plane (y,z), one derives the effective dimensionless one-dimensional coupled GPEs,

$$i\frac{\partial\psi_k}{\partial t}=\left[-\rho_k\frac{\partial^2}{\partial x^2}+\frac{1}{4\rho_k}\Omega_k^2x^2+u_k|\psi_k|^2+u_{12}|\psi_{3-k}|^2\right]\psi_k. \tag{5}$$

Here, the physical variables are rescaled as $t\to\omega_1^{-1}t$, $x\to b_0x$ $(b_0=\sqrt{\hbar/m_1\omega_1})$, and $\psi_k\to\sqrt{N/b_0}\psi_k$. Other dimensionless parameters become $\rho_k\equiv\frac{1}{2}\frac{m_1}{m_k}$, $\Omega_k\equiv\frac{\omega_k}{\omega_1}$, $u_k=\frac{m_1b_0a_kN}{m_kb_{k\perp}^2}$, and $u_{12}=\frac{2m_1b_0a_{12}N}{m_{12}(b_{1\perp}^2+b_{2\perp}^2)}$. The normalization for mean-field wave functions ψ_k are $\int dx|\psi_k|^2=N_k/N$. The Lagrangian of the system can be written as

$$L=\int dx\left\{\sum_{k=1}^{2}\left[\frac{i}{2}\left(\psi_k\frac{\partial\psi_k^*}{\partial t}-\psi_k^*\frac{\partial\psi_k}{\partial t}\right)+\rho_k\left|\frac{\partial\psi_k}{\partial x}\right|^2+\frac{1}{4\delta_k}\Omega_k^2x^2|\psi_k|^2+\frac{u_k}{2}|\psi_k|^4\right]+u_{12}|\psi_1|^2|\psi_2|^2\right\}, \tag{6}$$

where the asterisk denotes a complex conjugate. Equations (5) and (6) are the basic models describing the dynamics of the two-component condensates in the mean-field approximation. It is important to note that the present paper is focused on the case of BECs with weak interaction. In the general case, however, the two-components BECs in the one-dimensional (1D) system should be described by coupled nonpolynomial Schrödinger equations [14].

III. HARMONIC GENERATION AND NONLINEAR MODE COUPLING

A. Variational analysis

In order to provide physical insights into the dynamics of the condensates in the trapping potentials, we first give a theoretical prediction for the dynamics of the system by the variational method [33]. So, the Gaussian wave functions are considered to characterize the ground states, i.e., we take

$$\psi_k(x,t)=A_k\exp\left[-\frac{(x-x_k)^2}{2R_k^2}+i\alpha_kx+i\beta_kx^2\right]. \tag{7}$$

At a given time t, these functions define the Gaussian distributions centered at the positions x_k with half-widths R_k. The other variational parameters A_k (amplitude), α_k (velocity), and β_k (inverse square root of the beam curvature radius) are also time-dependent.

Substituting Eq. (7) into Eq. (6), we obtain the variational Lagrangian

$$L=\sum_{k=1}^{2}N_k\left[(\dot{\alpha}_k+4\rho_k\alpha_k\beta_k)x_k+\left(\dot{\beta}_k+4\rho_k\beta_k^2+\frac{1}{4\rho_k}\Omega_k^2\right)\times\left(\frac{R_k^2}{2}+x_k^2\right)+\frac{\rho_k}{2R_k^2}+\frac{u_kN_k}{2\sqrt{2\pi}NR_k}+\rho_k\rho_k^2\right]+\frac{u_{12}N_1N_2}{\sqrt{\pi}N\sqrt{R_1^2+R_2^2}}\times\exp\left[-\frac{(x_1-x_2)^2}{R_1^2+R_2^2}\right]. \tag{8}$$

Applying the Euler-Lagrangian equations $\frac{\partial L}{\partial Q_k}-\frac{d}{dt}\frac{\partial L}{\partial\dot{Q}_k}=0$, where $Q_k\equiv\{x_k,R_k,\alpha_k,\beta_k\}$, we obtain

$$N_k\left[\dot{\alpha}_k+4\rho_k\alpha_k\beta_k+2x_k\left(\dot{\beta}_k+4\rho_k\beta_k^2+\frac{1}{4\rho_k}\Omega_k^2\right)\right]-\frac{2u_{12}N_1N_2(x_k-x_j)}{\sqrt{\pi}N(R_1^2+R_2^2)^{3/2}}\exp\left[-\frac{(x_1-x_2)^2}{R_1^2+R_2^2}\right]=0, \tag{9}$$

$$N_k\left[\left(\dot{\beta}_k+4\rho_k\beta_k^2+\frac{1}{4\rho_k}\Omega_k^2\right)R_k-\left(\frac{\rho_k}{R_k}+\frac{u_kN_k}{2\sqrt{2\pi}N}\right)\frac{1}{R_k^2}\right]-\frac{u_{12}N_1N_2R_k}{\sqrt{\pi}N(R_1^2+R_2^2)^{3/2}}\left[1-\frac{2(x_1-x_2)^2}{R_1^2+R_2^2}\right]\exp\left[-\frac{(x_1-x_2)^2}{R_1^2+R_2^2}\right]=0, \tag{10}$$

$$\dot{x}_k=4\rho_k\beta_kx_k+2\rho_k\alpha_k, \tag{11}$$

$$R_k\dot{R}_k + 2x_k\dot{x}_k = 4\rho_k\alpha_k x_k + 4\rho_k\beta_k R_k^2 + 8\rho_k\beta_k x_k^2. \quad (12)$$

From Eqs. (9)–(12), one can obtain the evolution equations of all variational parameters. The equations for the center-of-mass coordinates and widths of the condensates are

$$\ddot{x}_k = -\Omega_k^2 x_k + \frac{4\rho_k u_{12} N_{3-k}(x_k - x_{3-k})}{\sqrt{\pi}N(R_1^2 + R_2^2)^{3/2}} \exp\left[-\frac{(x_1 - x_2)^2}{R_1^2 + R_2^2}\right], \quad (13)$$

and

$$\ddot{R}_k = -\Omega_k^2 R_k + \frac{4\rho_k^2}{R_k^3} + \sqrt{\frac{2}{\pi}}\frac{\rho_k u_k N_k}{N R_k^2} + \frac{4\rho_k u_{12} N_{3-k} R_k}{\sqrt{\pi}N(R_1^2 + R_2^2)^{3/2}} \times \left[1 - \frac{2(x_1 - x_2)^2}{R_1^2 + R_2^2}\right] \exp\left[-\frac{(x_1 - x_2)^2}{R_1^2 + R_2^2}\right]. \quad (14)$$

These are a set of four coupled nonlinear ordinary differential equations describing the evolution of the center and width of each condensate. The last terms in the right-hand side of both Eqs. (13) and (14) describe the intercomponent interaction and nonlinear coupling between the centers and the widths of the two condensates, respectively. Although the dipole oscillations are independent of the intracomponent interaction because of Kohn's theorem in Eq. (13), the intercomponent interaction still plays an important role in understanding the underlying physics of this situation. On the other hand, the second term in the right-hand side of Eq. (14) represents the dispersion of the background, which tends to spread the wave packet, and the third one is related to the interatomic interaction in a single condensate. Note that the corresponding 3D dynamical equations of Eqs. (13) and (14) were derived in Ref. [2] and the low lying excitation modes were discussed. As is clearly shown below, except the low lying modes obtained in Ref. [2], Eqs. (13) and (14) describe very rich dynamics, including the high harmonic generation, the nonlinear modes coupling, and the beating phenomenon, which are not presented in Ref. [2].

For simplicity, we consider two condensates constituting from different hyperfine spin states of ^{87}Rb, which are the $|F=1,\ m_f=-1\rangle$ and $|F=2,\ m_f=1\rangle$ states, respectively. It is noted that the magnetic trapping potentials have the same shape for these two states because the corresponding Landé g factors are also equal in modulus and have opposite sign. So for the external potentials, we have $\omega_1=\omega_2\equiv\omega$ and $\omega_{1\perp}=\omega_{2\perp}\equiv\omega_\perp$. For simplicity, we consider the case of two fixed intracomponent interactions and an alterable intercomponent interaction. Let us set the scattering lengths $a_1=a_2=5.36$ nm, and the atom numbers $N_1=N_2=10^4$. We choose the trapping frequencies $\omega=59$ Hz and $\omega_\perp=10\omega$ [3]. Under these assumptions, we have $\rho_1=\rho_2=\frac{1}{2}$, $\Omega_1=\Omega_2=1$, and $R_1=R_2\equiv R$. Expanding the width as $R=R_0+R'$ $(R'\ll R_0)$, where R' expresses a small departure from the equilibrium width R_0, defining the relative position between the two condensates as $l\equiv x_1-x_2$, and under weak excitation $|l|\ll R_0$, Eq. (13) can be reduced to (omitting the higher order terms)

$$\ddot{l} = -\omega_0^2 l - \frac{u_{12}}{2\sqrt{2\pi}R_0^5} l^3, \quad (15)$$

with $\omega_0^2=1-\frac{u_{12}}{\sqrt{2\pi}R_0^3}$. This is a nonlinear ordinary differential equation describing the oscillation of the two condensates center. From Eq. (15), one can easily find that l oscillates with frequency ω_r which depends on the initial excitation amplitude $l_0=x_{10}-x_{20}$ through

$$\omega_r^2 = \omega_0^2\left(1 + \frac{3u_{12}l_0^2}{16\sqrt{2\pi}\omega_0^2 R_0^5}\right). \quad (16)$$

It is clear that ω_r increases with initial driving amplitude l_0 and the intercomponent interaction a_{12}.

In order to discuss the dynamics of the widths of the condensates, applying the similar method as obtaining Eq. (15), Eq. (14) can also be simplified to

$$\ddot{R}' = -\omega_w^2 R' - \frac{3u_{12}}{4\sqrt{2\pi}R_0^4} l^2 + \frac{5u_{12}}{16\sqrt{2\pi}R_0^6} l^4, \quad (17)$$

with $\omega_w^2=1+\frac{3}{R_0^4}+\frac{u_k+u_{12}}{\sqrt{2\pi}R_0^3}$. This equation represents a forced linear pendulum oscillating with natural frequency ω_w. The last two terms in the right-hand side of the equation can be regarded as the forced terms induced by the oscillation of the two condensates' relative position. When the scattering length a_{12} is small, the forced terms in Eq. (17) can be ignored, the equation reduces to the harmonic pendulum and the width of the condensate oscillating with natural frequency ω_w. When the value of a_{12} becomes large enough, Eq. (17) indicates that the excitation spectrum can be modified by the forced terms, and the frequencies such as $2\omega_r, 4\omega_r, \ldots$ may appear in the spectrum of the width. It is also possible to generate resonance when the frequency of the driving force $2\omega_r$ is equal or very close to the intrinsic frequency ω_w, and the beating for the oscillation of the width will be excited. The beating frequency is $|2\omega_r-\omega_w|$.

Similar to Eq. (17), the forced oscillating equations describing the motion of the center of condensates can also be obtained,

$$\ddot{x}_k = -x_k + \frac{u_{12}}{2\sqrt{2\pi}R_0^3}\left(l - \frac{l^3}{2R_0^2} - \frac{3lR'}{R_0} + \frac{6lR'^2}{R_0^2}\right). \quad (18)$$

It is clear that when the interaction a_{12} is small, each condensate oscillates with its intrinsic frequency $\Omega=1/(2\pi)$; but when the value of the interaction a_{12} is increased, the higher-harmonic modes and the mixed modes will be excited, the frequencies such as $3\omega_r, 5\omega_r, \ldots$ and $\omega_r\pm\omega_w$, $\omega_r\pm 2\omega_w, \ldots$ may appear in the spectra for the motion of the centers. Equation (18) also indicates that, as the forcing frequency ω_r close to the intrinsic frequency $\Omega=1/(2\pi)$, the beating structures for oscillation of centers with frequency $|\omega_r-\Omega|$ will be excited.

In brief summary, our variational results show that, except the intrinsic modes ω_r and ω_w, the harmonic modes with frequency $2\omega_r, 3\omega_r, \ldots$, the mixed modes with frequency $\omega_r\pm\omega_w$, $\omega_r\pm 2\omega_w, \ldots$, and the beating modes with fre-

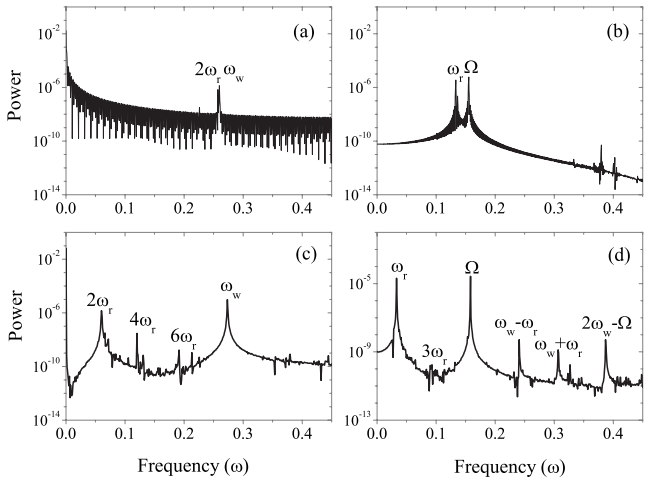

FIG. 1. Numerical results of the frequency spectra for the oscillation of the width $\langle R_1 \rangle$ [left panels (a) and (c)] and center $\langle x_1 \rangle$ [right panels (b) and (d)]) with a small value of a_{12} [top panels (a) and (b): $a_{12}=1.0$ nm] and a large one [bottom panels (c) and (d): $a_{12}=5.0$ nm], respectively.

quency $|2\omega_r-\omega_w|$ and $|\omega_r-\Omega|$ can be excited in the system. These analytical predictions will be confirmed by the direct numerical simulations.

B. Direct numerical results of the coupled GPEs

To confirm the above variational predictions, we have performed a direct numerical simulation of the fully coupled GPEs (5). The coupled GPEs (5) are integrated numerically by means of the fourth-order Runge-Kutta scheme in time along with a second-order finite-difference discretization in space [34]. As is shown in [34], this numerical method is stable and accurate to integrate the time-dependent GPEs. Initially, we search the equilibrium solution of two-component BECs by time propagation of Eq. (5). Starting from this initial state with a small displacement of the relative positions of the two confining traps, the fully coupled GPEs (5) are integrated and the collective excitations in the system can be obtained. Some of our numerical results are presented in Figs. 1 and 2. Figure 1 shows the spectra for the motion of the center of the condensate and its width, respectively. It is noted that the center-of-mass coordinate and the width of the condensate in simulations are defined as $\langle x \rangle = \int_{-\infty}^{+\infty} x|\psi|^2 dx$ and $\langle R \rangle^2 = \int_{-\infty}^{+\infty} (x-\langle x \rangle)^2 |\psi|^2 dx$, respectively. The spectra shown in Fig.1 are obtained by performing a frequency analysis for the motion of the center of the condensate and its width. The harmonic frequencies and the mixed frequencies are clearly shown in Fig. 1. The spectrum shows that two major frequencies for the oscillation of width exist under small scattering length a_{12} [Fig. 1(a)]: the intrinsic frequency ω_w and the driving frequency $2\omega_r$. Furthermore, the spectrum for the width shows several even double frequencies (such as $2\omega_r, 4\omega_r, \ldots$) when a_{12} becomes large [Fig. 1(c)]. The spectra for the motion of the center [Figs. 1(b) and 1(d)] have similar properties; but for the center, in addition to odd double frequencies (such as $3\omega_r, 5\omega_r, \ldots$), there are several mixed frequencies ($\omega_r \pm \omega_w, \ldots$) for larger values of a_{12} [Fig. 1(d)]. These excited modes shown in Fig. 1 are in good agreement with our variational predictions.

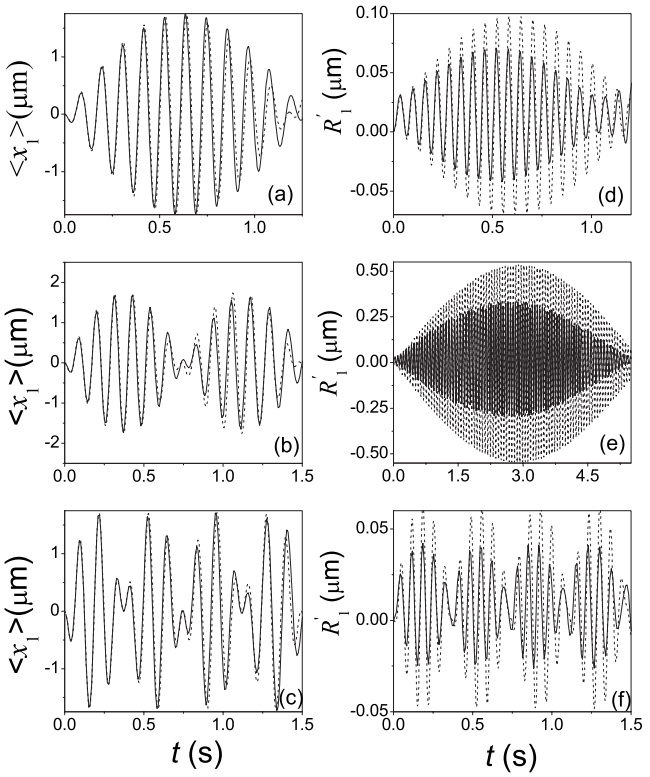

FIG. 2. The beating structures for the center $\langle x_1 \rangle$ (left panels) and width $R_1'=R_0-\langle R_1 \rangle$ (right panels) at different scattering length a_{12}. (a) and (d) $a_{12}=0.5$ nm; (b) and (e) $a_{12}=0.84$ nm; (c) and (f) $a_{12}=1.8$ nm. The solid and dashed lines, respectively, correspond to the direct numerical results and the variational results.

The beating structures induced by the nonlinear modes coupling can also be revealed, which are shown in Fig. 2 for small scattering lengths. In Fig. 2, both the variational results of Eqs. (15)–(18) (dashed line) and the direct numerical results of Eqs. (5) (solid line) are presented. It is clear that the variational results are in good agreement with the direct numerical results, especially for the motion of the center and the frequency of excited modes. We also can see that the beating frequency for oscillating of the center increases with a_{12} [Figs. 2(a)–2(c)] and it has the minimum value when $a_{12} \approx 0$ [Fig. 2(a)]. The beating frequency for the width has the minimum value at $a_{12} \approx 0.84$ nm [Fig. 2(e)].

IV. PARAMETRIC RESONANCE AND FORMATION OF MULTISOLITON CONFIGURATIONS

In this section, we aim to study the parametric resonance in a mixture of two BECs by modulating the scattering length a_{12} periodically as

$$\bar{a}_{12} = a_{12}[1 + \varepsilon \cos(\nu t)],$$

i.e.,

$$\bar{u}_{12} = u_{12}[1 + \varepsilon \cos(\nu t)]. \tag{19}$$

Here, $\bar{a}_{12}$ ($\bar{u}_{12}$) is the modified scattering length (interaction) with an additional modulation term $a_{12}\varepsilon \cos(\nu t)$, ε and ν being the amplitude and frequency of the time-dependent modulation, which can be carried out by means of the Feshbach resonance [32]. The Feshbach resonance allows one to switch the interatomic interaction periodically in time, and will undoubtedly open the door for the study of the matter-wave management in multicomponent BECs.

A. Theoretical prediction

Again we first give a theoretical prediction for the appearance of the parametric resonance in two-component BECs by using the variational result of Eq. (15). It should be noted that in obtaining the variational results of Eqs. (13)–(15), the atoms interaction expressed by $u_{1(2)}$ and u_{12} can either be time-independent or time-dependent. On the other hand, the variational results of Eqs. (13)–(15) are not changed if $u_{1(2)}$ and u_{12} are time-dependent. Because in the initial stage of the parametric resonance, the excitation is weak, i.e., $|l| \ll R_0$, Eq. (15) can be simplified to

$$\ddot{l} = -\left(1 - \frac{u_{12}}{\sqrt{2\pi}R_0^3}\right) l. \tag{20}$$

Using Eq. (19), Eq. (20) can be reduced to the well-known Mathieu's equation [35]

$$\ddot{l} = -\omega_0^2[1 - \gamma \cos(\nu t)]l, \tag{21}$$

where $\gamma = \frac{u_{12}\varepsilon}{\sqrt{2\pi}R_0^3\omega_0^2}$. It is also well-known that the parametric resonance can take place in the system if the frequency of the driving force ν meets the following condition [35]

$$\nu = \frac{2\omega_0}{n}, \tag{22}$$

where $n = 1, 2, 3, \ldots$ denotes the order number of the resonances. The resonance boundaries for the lower-order resonances are given by

$$n = 1: \frac{\nu}{2\omega_0} = 1 \pm \frac{1}{4}\gamma, \tag{23}$$

$$n = 2: \frac{\nu}{\omega_0} = 1 - \frac{1}{4}\gamma^2, \quad \frac{\nu}{\omega_0} = 1 + \frac{1}{24}\gamma^2, \tag{24}$$

$$n = 3: \frac{\nu}{2\omega_0} = \frac{1}{3}\left[1 - \frac{1}{64}\gamma^2 \pm \frac{81}{1024}\gamma^3\right]. \tag{25}$$

That is, if the parameters are selected in the range given by one of Eqs. (23) or (24), the parametric resonance will be excited in the system.

B. Direct numerical simulation of the parametric resonance

The theoretical results given by Eqs. (22)–(25) just predict the conditions for appearance of the parametric resonance in the system. We can expect that very rich dynamical phenomena would be excited when the parametric resonance takes place. It is clear that this cannot be predicted by the above theoretical method, thus a fully numerical simulating of the coupled GPEs (5) is needed. So we present the complete process of the parametric resonance in two-component BECs by direct numerical simulation of the full GPEs (5). In numerical integrating of the GPEs (5), the scattering length between different components is varied according to Eq. (19). The parameters in Eq. (19) are adjusted into the unstable region as described by Eq. (23): the scattering length $a_{12}=2.5$ nm, the external driving frequency $\nu/2\omega_0=1.0$, and the driving amplitude $\varepsilon=0.5$. The numerical results are shown in Figs. 3–10.

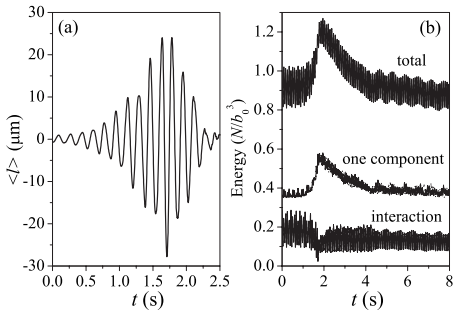

FIG. 3. Variation of the relative position of the two condensates (a) and the corresponding energies of the system (including the total energy, the energy of each component, and the interaction energy between the two condensates)(b).

It is clear from Fig. 3(a) that the amplitude of the oscillation of the relative position of the two condensates increases gradually and reaches a maximum value at $t \simeq 1.66$ s, i.e., the parametric resonance is induced. Figure 3(b) indicates that the total energy and the energy of each component also increase gradually, while the interactive energy contrarily decreases until $t=1.66$ s. The minimum value of the interaction energy demonstrates the largest phase separation for the two condensates. Because of large amplitude oscillation induced by the resonance, the dark soliton trains can be excited, which are shown in Fig. 4. The dark solitons repel each other and oscillate in the trap. It is noted that the generation of the dark soliton trains is not caused by the modulational instability because the condition of the modulational instability is not satisfied, i.e., $[(a_{12})_{\max}]^2 < a_1 a_2$, where $(a_{12})_{\max} = a_{12}(1+\varepsilon) = 3.75$ nm.

In order to observe the mechanism of formation of the soliton trains clearly, we also show the evolution of the density distributions for the two condensates at different times in Figs. 4(a)–4(f). Figure 4(a) gives the two initial density profiles. Before $t=1.59$ s, the phase separation of the two condensates happens periodically. The compression and expansion of the wave packets occur periodically with the period of the external modulation. We can see that the wave packets at $t=1.59$ s are compressed to almost half of the initial density distributions [Fig. 4(b)]. The distance between the centers of the two-condensates reaches 30 μm at $t=1.66$ s [Fig. 4(c)], the two condensates separate completely. The two wave packets vary dramatically in the interface of the two

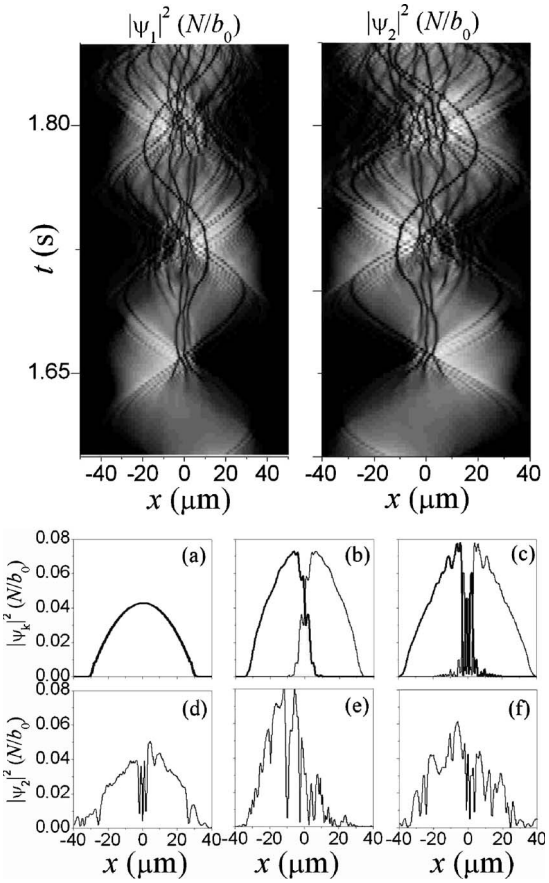

FIG. 4. (Top) The contour plots of the densities during the parametric resonance with $a_{12}=2.5$ nm and $\varepsilon=0.5$. (Bottom) The density profiles of $|\psi_1|^2$ (thin curve) and $|\psi_2|^2$ (thick curve) at different evolution times: (a) $t=0$ s, (b) $t=1.59$ s, (c) $t=1.66$ s, (d) $t=1.691$ s, (e) $t=1.738$ s, and (f) $t=1.755$ s.

condensates, and the wave packets break up due to dynamical instability, which is induced by strong interaction between the packets. Under the competition between the nonlinearity and the dispersion, three dark solitons are formed at $t=1.66$ s [Fig. 4(c)]. Then, the three solitons oscillate around $x=0$ [Figs. 4(d)–4(f)], to make clear, only the profile of $|\psi_1|^2$ is shown in Figs. 4(d)–4(f). The oscillating of the three solitons can also be clearly seen in the contour plots of the densities shown in Fig. 4 (top panels). Henceforth, the strong interaction between two-condensates takes place periodically and multisolitons are excited successively. The evolution of the multidark solitons are shown in Fig. 4 (top panels).

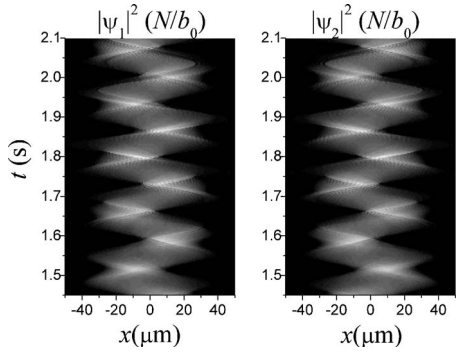

FIG. 5. The periodic phase separation of two-component BECs when the modulation is cut off before formation of soliton trains (at $t=1.59$ s).

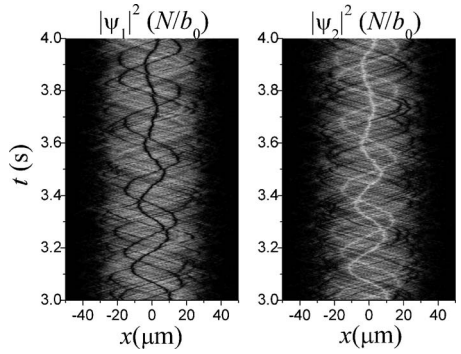

FIG. 6. Long lived dark-dark and bright-bright soliton pairs when the modulation is cut off after formation of soliton trains.

From the above discussion we can conclude that the nonlinear resonance interaction of the two-condensates induced by periodic modulation of intercomponent scattering length results in generation of multisolitons. It is clear that this mechanism for exciting solitons in BECs is different from that discussed in Refs. [30,31]. In Ref. [30], a set of moving

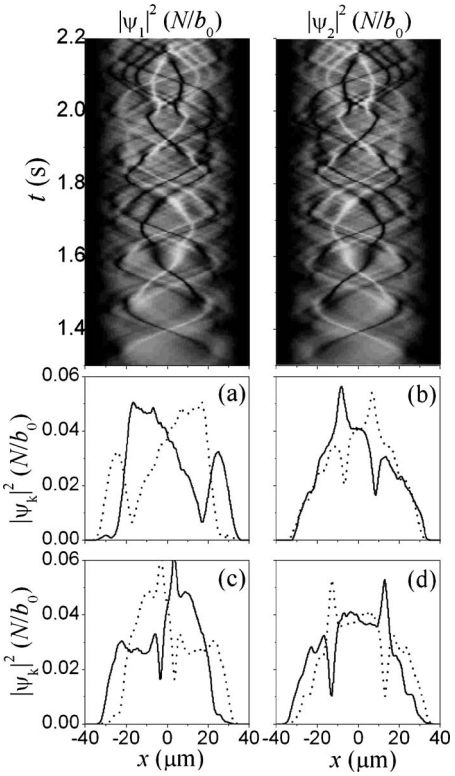

FIG. 7. (Top) The contour plots of the densities with $a_{12}=4.5$ nm and $\varepsilon=0.18$. (Bottom) The density profiles at different times: (a) $t=1.352$ s; (b) $t=1.379$ s; (c) $t=1.404$ s; and (d) $t=1.425$ s. (The thin curve and the thick one represent $|\psi_1|^2$ and $|\psi_2|^2$, respectively.)

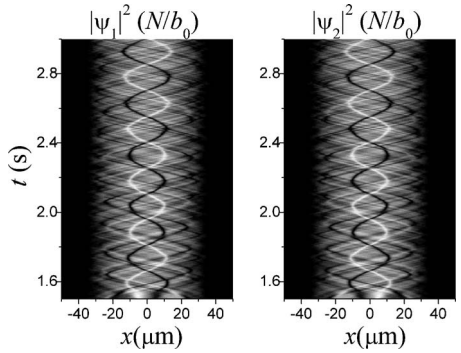

FIG. 8. Long lived dark-bright soliton pairs when the modulation is stopped after the dark-bright soliton pairs are excited at $t=1.514$ s.

fundamental solitons was generated from the prescribed higher-order soliton states by an extremely weak periodic modulation of the scattering length in an attractive one-component BEC. In Ref. [31], solitons were produced from the linear states via the adiabatic temporal varying the scattering length in one-component BEC. It is interesting to note that a single soliton can be generated by the method discussed in Ref. [31]. Nonlinear resonance interaction of two-condensates, however, makes the excitations in two-component BECs more complicated and it results in rich dynamics in two-component BECs (as is shown below).

Further investigation shows that some interesting phenomena can occur if we stop the modulation of the interaction constant a_{12} [i.e., setting $\varepsilon=0$ in Eq. (19)] before/after formation of soliton trains. Cutting off the modulation of the interaction constant a_{12} before formation of the dark soliton trains ($t=1.59$ s in Fig. 4), we find that periodic phase separation of two condensates and periodic compression and expansion of the wave packets take place. These can be clearly seen from the contour plots of the densities shown in Fig. 5. It is noted that a similar effect of the periodic phase separation of the two-condensates was reported in Ref. [36]. It is clear that the mechanism exciting the phase separation discussed in Ref. [36] is different from that presented in this paper. In Ref. [36], the periodic phase separation of the two-condensates is driven by a linear coupling of the two-condensates (induced by means of a resonant electromagnetic spin-flipping field). To keep the periodic phase separation of the two-condensates, persistent linear coupling between the two-condensates should be applied. Meanwhile, as was shown in Ref. [36], the interaction between the two-condensates is very weak, the two-condensates just perform oscillating of their positions, periodically passing through each other. In the present work, however, the persistent phase separation is excited by the nonlinear resonant interaction of the two-condensates (induced by periodic modulation of the intercomponent scattering length) and the two-condensates exhibit strong interaction as they oscillate. Furthermore, as the phase separation is excited, it will keep a long time even if the modulation of the intercomponent scattering length is cut off.

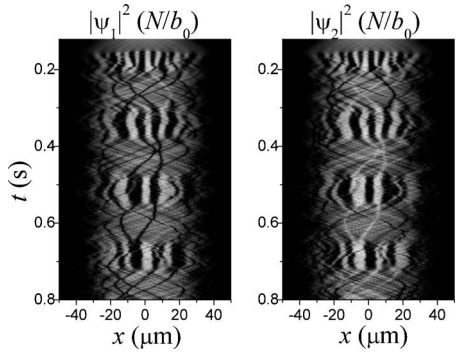

FIG. 9. Periodic excitation of multidomain walls under modulation with $a_{12}=5.0$ nm and $\varepsilon=0.5$.

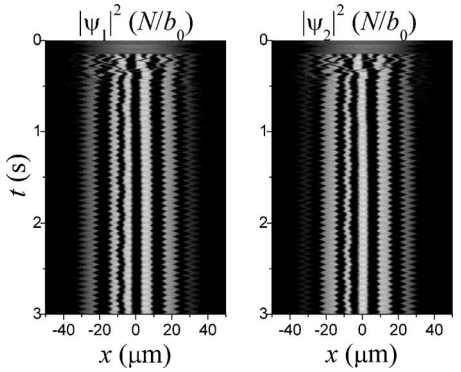

FIG. 10. Long lived domain walls when removing the modulation after the domain walls are generated.

If we stop the modulation of the interaction after formation of the dark soliton trains (at $t=1.68$ s), the excited soliton trains can keep a very long time until a new equilibrium soliton state at $t=3$ s is formed. In Fig. 6 we illustrate the evolution of the soliton state after $t=3$ s. It is found that the dark-dark soliton pair in one condensate and the bright-bright soliton pair in another condensate are formed, instead of the structure of the dark soliton trains. We believe this equilibrium structure results from the incessant interaction between two condensates for small intercomponent interaction a_{12}.

When we increase the value of the interaction to $a_{12}=4.5$ nm and decrease the modulation amplitude to $\varepsilon=0.18$, the bright-dark soliton pairs in each component can be created. We should note that, in this case, the modulational instability condition is still not satisfied, i.e., $[(a_{12})_{\max}]^2 < a_1 a_2$, where $(a_{12})_{\max}=a_{12}(1+\varepsilon)=5.31$ nm. So, the formation of the bright-dark soliton pairs is also not caused by the modulational instability. The contour plots of the density profiles are illustrated in Fig. 7. We can see that the dark-bright soliton pairs are generated both in each condensate and between the two condensates. That is, in the place where the dark soliton is formed in one component, the bright soliton is formed in another one [Figs. 7(a)–7(d)]. The dark-bright soliton pairs are generated at $t=1.379$ s [Fig. 7(b)] by a large density disturbance between two condensates [Fig. 7(a)]. Then the soliton pairs oscillate around $x=0$ [Figs. 7(b)–7(d)]. Compared with the previous case, there are two points that need to be mentioned. First, the amplitude ε is

small, and the parametric excitation becomes weak, so the whole phase separation between the two-condensates cannot occur. Secondy, the interaction between the condensates increases due to the larger scattering length a_{12}. For the weak excitation, the local density distributions of the condensates are disturbed largely, and the local phase separation occurs, leading to the generation of dark-bright soliton states. In Ref. [23], the generation of soliton trains is induced by local density disturbance in BEC. Obviously, the generation mechanism of such a soliton pair is similar with that discussed in Ref. [23], but different with the previous case (dark-dark soliton pair and bright-bright soliton pair) for a small interaction.

Once the dark-bright soliton pairs are excited, we stop the modulation of the intercomponent scattering length at $t=1.514$ s, as is shown in Fig. 8, the soliton pairs can keep a very long time and the lifetime exceeds about $t=3$ s.

There are other multisoliton configurations which can be generated by the parametric resonance, e.g., formation of multiple domains [18,19]. In our system, when we increase the value of the interaction ($a_{12}=5.0$ nm) and the amplitude of the periodical modulation ($\varepsilon=0.5$), the periodic generation of multidomain walls can take place, which is shown in Fig. 9. The domain walls appear alternately due to the periodical modulation. As we know, the formation of a domain wall is related to the modulational instability in two-component BECs. In half of the modulation period, the condition of the modulational instability is satisfied ($a_{12}>\sqrt{a_1 a_2}$) and the domain walls can be formed. In another half of the period, the condition cannot be satisfied and the domain walls disappear.

The most interesting thing is that when we remove the modulation of the interaction constant a_{12} during the formation of the multiple domains, the excited domain walls can keep a very long time (Fig. 10). It is clear that the condition of the modulational instability is not satisfied when we set $\varepsilon=0$. We believe that this result needs to be discussed theoretically in the future.

V. CONCLUSIONS

In conclusion, the collective dynamics of two-component BECs described by the two coupled Gross-Pitaevskii equations are investigated by means of the variational analysis and direct numerical simulation. The collective dynamics of two-component BECs under the parameter excitation are discussed. The harmonic generation and the nonlinear modes coupling are revealed in the system. Subsequently, the parametric resonance in two-component BECs by modulating the intercomponent interaction is investigated. The resonance conditions in terms of the modulation frequency and the strength of interspecies interaction are obtained. The formation of multisoliton states in the system are discussed, in particular, a method for creation of multisoliton configurations in two-component BECs by modulating the parameter of the system is presented.

The results presented in this work can be observed easily in experiments. The two-component BECs can be prepared like the experiment described in Ref. [3]. To observe the harmonic generation and nonlinear modes coupling, the excitations can be induced by the displacement of the relative positions of the confining traps; and for the parametric resonance and formation of the multisoliton configurations, the modulation of the atomic scattering length of different components can be implemented by using the so-called Feshbach resonance technique [32]. We hope our results will stimulate the experiment in this direction.

ACKNOWLEDGMENTS

This work was supported by the National Natural Science Foundation of China under Grant Nos. 10774120 and 10475066, by the Natural Science Foundation of Gansu Province under Grant No. 3ZS051-A25-013, and by Creation of Science and Technology of Northwest Normal University, China, under Grant No. NWNU-KJCXGC-03-17.

[1] H. Pu and N. P. Bigelow, Phys. Rev. Lett. **80**, 1134 (1998).
[2] Th. Busch, J. I. Cirac, V. M. Pérez-García, and P. Zoller, Phys. Rev. A **56**, 2978 (1997).
[3] D. S. Hall, M. R. Matthews, J. R. Ensher, C. E. Wieman, and E. A. Cornell, Phys. Rev. Lett. **81**, 1539 (1998); D. S. Hall, M. R. Matthews, C. E. Wieman, and E. A. Cornell, *ibid.* **81**, 1543 (1998).
[4] P. Maddaloni, M. Modugno, C. Fort, F. Minardi, and M. Inguscio, Phys. Rev. Lett. **85**, 2413 (2000).
[5] G. Modugno, M. Modugno, F. Riboli, G. Roati, and M. Inguscio, Phys. Rev. Lett. **89**, 190404 (2002).
[6] A. Sinatra, P. O. Fedichev, Y. Castin, J. Dalibard, and G. V. Shlyapnikov, Phys. Rev. Lett. **82**, 251 (1999).
[7] K. Kasamatsu, M. Tsubota, and M. Ueda, Phys. Rev. A **69**, 043621 (2004).
[8] P. Öhberg and L. Santos, Phys. Rev. Lett. **86**, 2918 (2001).
[9] Th. Busch and J. R. Anglin, Phys. Rev. Lett. **87**, 010401 (2001).
[10] M. Víctor Pérez-García and Vadym Vekslerchik, Phys. Rev. E **67**, 061804 (2003); G. D. Montesinos, V. M. Pérez-García, and H. Michinel, Phys. Rev. Lett. **92**, 133901 (2004).
[11] P. G. Kevrekidis, H. E. Nistazakis, D. J. Frantzeskakis, A. Boris Malomed, and R. Carretero-González, Eur. Phys. J. D **28**, 181 (2004); S. K. Adhikari, Phys. Lett. A **346**, 179 (2005).
[12] P. G. Kevrekidis, H. Susanto, R. Carretero-Gonzalez, B. A. Malomed, and D. J. Frantzeskakis, Phys. Rev. E **72**, 066604 (2005).
[13] V. A. Brazhnyi and V. V. Konotop, Phys. Rev. E **72**, 026616 (2005).
[14] Luca Salasnich and Boris A. Malomed, Phys. Rev. A **74**, 053610 (2006).
[15] J. Babarro, M. J. Paz-Alonso, H. Michinel, J. R. Salgueiro, and D. N. Olivieri, Phys. Rev. A **71**, 043608 (2005).
[16] V. M. Pérez-García and J. B. Beitia, Phys. Rev. A **72**, 033620

(2005).
[17] Ju-Kui Xue, Phys. Rev. E **73**, 028601 (2006).
[18] M. Trippenbach, Krzysztof Góral, Kazimierz Rzażewski, B. A. Malomed, and Y. B. Band, J. Phys. B **33**, 4017 (2000); A. B. Malomed, H. E. Nistazakis, D. J. Frantzeskakis, and P. G. Kevrekidis, Phys. Rev. A **70**, 043616 (2004).
[19] Stéphane Coen and Marc Haelterman, Phys. Rev. Lett. **87**, 140401 (2001).
[20] P. G. Kevrekidis, A. B. Malomed, D. J. Frantzeskakis, and A. R. Bishop, Phys. Rev. E **67**, 036614 (2003).
[21] K. Kasamatsu and M. Tsubota, Phys. Rev. Lett. **93**, 100402 (2004).
[22] J. Denschlag, J. E. Simsarian, D. L. Feder, C. W. Clark, L. A. Collins, J. Cubizolles, L. Deng, E. W. Hagley, K. Helmerson, W. P. Reinhart, S. L. Rolston, B. I. Schneider, and W. D. Phillips, Science **287**, 97 (2000); B. Wu, J. Liu, and Q. Niu, Phys. Rev. Lett. **88**, 034101 (2002).
[23] Z. Dutton, M. Budde, C. Slowe, and L. V. Hau, Science **293**, 663 (2001).
[24] J. J. García-Ripoll, V. M. Pérez-García, and P. Torres, Phys. Rev. Lett. **83**, 1715 (1999).
[25] B. Baizakov, G. Filatrella B. Malomed, and M. Salerno, Phys. Rev. E **71**, 036619 (2005).
[26] P. G. Kevrekidis, G. Theocharis, D. J. Frantzeskakis, and A. B. Malomed, Phys. Rev. Lett. **90**, 230401 (2003); H. Saito and M. Ueda, *ibid.* **90**, 040403 (2003).
[27] C. Tozzo, M. Krämer, and F. Dalfovo, Phys. Rev. A **72**, 023613 (2005); J. J. Garcia-Ripoll, V. M. Perez-Garcia, and P. Torres, Phys. Rev. Lett. **83**, 1715 (1999).
[28] S. K. Adhikari, J. Phys. B **36**, 1109 (2003).
[29] P. Engels, C. Atherton, and M. A. Hoefer, Phys. Rev. Lett. **98**, 095301 (2007); K. Staliunas, S. Longhi, and G. J. de Valcarcel, *ibid.* **89**, 210406 (2002).
[30] H. Sakaguchi and A. B. Malomed, Phys. Rev. E **70**, 066613 (2004).
[31] P. G. Kevrekidis, V. V. Konotop, A. Rodrigues, and D. J. Frantzeskakis, J. Phys. B **38**, 1173 (2005).
[32] S. Inouye, M. R. Andrews, J. Stenger, H.-J. Miesner, D. M. Stamper-Kurn, and W. Ketterle, Nature (London) **392**, 151 (1998); E. A. Donley, N. R. Claussen, S. L. Cornish, J. L. Roberts, E. A. Cornell, and C. E. Wieman, *ibid.* **412**, 295 (2001).
[33] V. M. Pérez-García, H. Michinel, J. I. Cirac, M. Lewenstein, and P. Zoller, Phys. Rev. Lett. **77**, 5320 (1996).
[34] L. D. Carr, M. J. Holland, and B. A. Malomed, J. Phys. B: At. Mol. Opt. Phys. **38**, 3217 (2005); Ju-Kui Xue, Eur. Phys. J. D **37**, 241 (2006).
[35] J. V. José and E. J. Saletan, *Classical Dynamics: A Contemporary Approach* (Cambridge University Press, Cambridge, England, 1998).
[36] I. M. Merhasin, B. A. Malomed, and R. Driben, J. Phys. B: At. Mol. Opt. Phys. **38**, 877 (2005).